remote sensing

MDPI

Article

Spectral Reflectance of Polar Bear and Other Large Arctic Mammal Pelts; Potential Applications to Remote Sensing Surveys

George Leblanc [1,*], Charles M. Francis [2,†], Raymond Soffer [1,†], Margaret Kalacska [3,†] and Julie de Gea [3,†]

1 Flight Research Laboratory, National Research Council of Canada, 1920 Research Rd., Ottawa, ON K1A 0R6, Canada; ray.soffer@nrc-cnrc.gc.ca
2 Canadian Wildlife Service, Environment Canada 1125 Colonel By, Ottawa, ON K1A 0H3, Canada; charles.francis@canada.ca
3 Department of Geography, McGill University, 805 Sherbrooke West, Montreal, QC H3A 0B9, Canada; margaret.kalacska@mcgill.ca (M.K.); juliedegea@gmail.com (J.d.G.)
* Correspondence: george.leblanc@nrc-cnrc.gc.ca; Tel.: +1-613-998-3525; Fax: +1-613-952-1704
† These authors contributed equally to this work.

Academic Editors: Susan L. Ustin, Magaly Koch and Prasad S. Thenkabail
Received: 6 November 2015; Accepted: 7 March 2016; Published: 25 March 2016

Abstract: Spectral reflectance within the 350–2500 nm range was measured for 17 pelts of arctic mammals (polar bear, caribou, muskox, and ringed, harp and bearded seals) in relation to snow. Reflectance of all pelts was very low at the ultraviolet (UV) end of the spectrum (<10%), increased through the visual and near infrared, peaking at 40%–60% between 1100 and 1400 nm and then gradually dropped, though remaining above 20% until at least 1800 nm. In contrast, reflectance of snow was very high in the UV range (>90%), gradually dropped to near zero at 1500 nm, and then fluctuated between zero and 20% up to 2500 nm. All pelts could be distinguished from clean snow at many wavelengths. The polar bear pelts had higher and more uniform averaged reflectance from about 600–1100 nm than most other pelts, but discrimination was challenging due to variation in pelt color and intensity among individuals within each species. Results suggest promising approaches for using remote sensing tools with a broad spectral range to discriminate polar bears and other mammals from clean snow. Further data from live animals in their natural environment are needed to develop functions to discriminate among species of mammals and to determine whether other environmental elements may have similar reflectance.

Keywords: polar bear; seal; spectral signature; muskox; caribou; hyperspectral

1. Introduction

Polar bears, *Ursus maritimus* are widespread throughout the Arctic, but, like many other Arctic animals, there are increasing concerns that their ecology and population dynamics are being negatively impacted by changes in Arctic ecosystems. The Arctic is undergoing rapid environmental change due to climate warming, which is leading to many changes in its ecosystem, including loss of multi-year sea ice and longer ice-free seasons [1]. These changes can directly affect polar bears through loss of hunting opportunities on sea ice, resulting in lower reproduction and higher risk of mortality [2,3]. Warming climates are also associated with increased shipping, development and other human activity in the arctic, which may increase the risk for human-bear conflicts.

Effective management of polar bear populations, including managing harvest, and mitigating threats due to environmental change, requires information on distribution and abundance of bears and how these are changing over time. Traditionally, the most widely used method for estimating

population size of polar bears has been with mark-recapture [4,5]. With this approach, polar bears are located, generally from a helicopter, sedated by darting, and then marked using a combination of ear tags and tattoos to ensure the marks are not lost [5]. By repeating captures in subsequent years, and assuming marked and unmarked animals are equally likely to be recaptured, standard open-population capture-recapture methods can be used to estimate population size and changes in population size [4].

Recently, aerial surveys have also been used for estimating population densities and distribution in parts of the Arctic [6–10]. Either fixed wing aircraft or helicopters can be flown along predetermined transects, with two or more observers recording all bears detected and their position in relation to the aircraft. With appropriate placement of transects, densities can be estimated using distance sampling methods. These approaches have been used in Hudson Bay during the ice free period in late summer [8], as well as on sea ice [10].

The traditional capture methods as well as aerial survey methods have a number of disadvantages, including high costs, significant risks to researchers, and cultural and ethical concerns about capturing bears. Low level aerial surveys, whether to capture or to count bears, are inherently risky, especially in the Arctic, where surveys may take place at long distances from available fuel and severe weather can increase risks—over the past 30 years, a number of researchers have been involved in aircraft accidents, including some fatalities [5]. Capturing and handling bears has additional risks, both to bears and to researchers, particularly if the sedative dose is incorrectly estimated. In addition, many native communities object to unnecessary handling and marking of bears and are advocating for survey methods that do not involve capturing animals.

Remote sensing technologies based on either airborne (manned or unmanned vehicles) or satellite imagery provide a potential alternative survey method for bears or other large mammals, particularly in arctic areas where there is little or no vegetation tall enough to hide large mammals from above [11]. One method that may provide a solution is high spatial resolution satellite imagery. Satellite imagery is rapidly decreasing in cost, and could potentially be used to survey large areas of the arctic, provided there are sufficient periods with adequate daylight and no cloud cover. Aerial photography is another possible solution as it can be flown at higher altitudes than conventional surveys, reducing risks, and could potentially be combined with flights undertaken for other purposes. Aerial photography has been used to count colonies of arctic-nesting geese since 1973 [12]. Seals have been surveyed with airborne imagery using a double sampling method: automated processing of thermal imagery to detect animals, combined with a manual examination of concurrent aerial photographs in the visual spectrum to identify species [13]. High spatial resolution satellite imagery has been used to estimate the size of a remote colony of king penguins [14] and to locate and survey Emperor Penguin colonies in Antarctica [15–17]. LaRue *et al.*, (2011) [17] compared counts of Weddell seals in Antarctica derived from high resolution satellite imagery with counts made from ground-based studies and found a strong correlation over time. Platanov *et al.*, (2013) [18] suggested that several species of mammals in the Russian Arctic, including walruses and polar bears (based on tracks) could potentially be detected from satellite imagery, though they did not have ground data to verify their conclusions. Stapleton *et al.*, (2014) [11] used high resolution panchromatic satellite imagery to count individual polar bears in a concentration area on a small island in the Foxe Basin in late summer when no snow or ice was present. They visually compared a satellite image when bears were present against reference images taken a few weeks apart to locate appropriate sized white objects that were not present on the other images and that likely represented bears. They found good correspondence with independent population estimates derived from aerial transect surveys undertaken at the same time.

Effective detection of polar bears from remote-sensing imagery, whether satellite-based or airborne, using any sort of automated process, requires being able to discriminate bears from both the background and from other large animals that might occur in similar habitats. For most of the year, when polar bears are on snow or ice, discriminating bears from the background using visible light presents a challenge because they appear basically white against a background of white snow

or ice. Subtle differences in shading can be detected with the human eye, with bears appearing more yellowish or orange compared to the more bluish shades of snow. However, these differences need to be quantified to support automated detection.

Polar bears can potentially be discriminated from snow more readily outside of the visible light range [19–21]. Polar bear fur is highly absorbent in the lower ultraviolet (UVA) region, in contrast to snow, and as such, when imaged in the UVA range, polar bears appear black against a white snow background [19,20,22]. Thermal infrared (TIR) (3000–12,000 nm) imaging has been used to survey a variety of arctic mammals, including walrus [23] and seals (e.g., [13]), and could potentially detect polar bears [21]. Early attempts to detect polar bears with thermal imaging met with limited success [24], but this was likely due to the limited sensitivity of the equipment used, given that subsequent studies have shown that exercising bears radiate heat several degrees warmer than the ambient temperatures [21]. Thermal imaging has been used in the field to detect denning polar bears under the snow [25]. The internal den temperature can be as high as 30 °C resulting in average surface temperatures over dens 10 °C higher than surrounding snow banks ([26] as cited in [27]). Even with this very large contrast in temperatures, and under favorable conditions, Amstrup *et al.*, (2004) [27] were only able to detect 83% of 23 known dens. Under less suitable conditions including bright sunlight, excessive blowing snow and fog, dens could not be reliably detected. Strong winds rapidly dissipate heat, reducing the thermal contrast [21], thus making either dens or individual bears more difficult to discriminate from background variation based on thermal imagery.

The goal of this study was to expand the previous work on polar bear detection via spectral means by measuring in more detail the reflectance spectra of bear pelts through a broader range of wavelengths as well as with finer spectral resolution. We measured the solar reflectance of polar bear pelts within the ultraviolet (UVA 350–400 nm), visible (VIS 400–700 nm), near infrared (NIR 700–1000 nm) and shortwave infrared (SWIR 1000–2450 nm) ranges and compared these both with snow and with the pelts of a variety of other arctic mammals: ringed (*Pusa hispida*), harp (*Pagophilus groenlandicus*) and bearded (*Erignatus barbatus*) seals; caribou (*Rangifer tarandus*); and muskox (*Ovibus moschatus*).

2. Materials and Methods

The data collection process consisted of acquiring spectral reflectance measurements in full sunlight in early afternoon of various museum pelts of polar bears and other mammal species, together with interspersed measurements of adjacent clean undisturbed snow and a 30.5 cm × 30.5 cm Spectralon™ reflectance standard calibration panel.

We measured reflectance using a portable ASD FieldSpec® 3 spectrometer of range 350–2500 nm and 1 nm sampling interval (Analytical Spectral Devices, Boulder, CO, USA). An 8° hemispherical fore-optic was used in conjunction with the spectrometer's fiber optic hand-held collection unit to take measurements from a vertical distance of approximately 25 cm above each measurement site. The combined effects of using the 8° hemispherical fore-optics and the 25 cm height provided a measurement area of approximately 14.5 cm^2, which ensured measurements were collected only over specific areas of the pelts, snow and the reflectance panel. The fiber optic cable of the collection unit was 1.2 m long and was attached to a camera stand that allowed approximately 1 m separation between the operator and the unit to reduce specular reflection from the operator [28]. The reflectance values of the targets of interest (pelts and undisturbed snow) were obtained as a result of standard processing practices (as implemented in ASD's standard processing software) using the ratio between the target signal and the Spectralon™ calibration panel signal which is then multiplied by the laboratory measured reflectance for that panel.

The ASD spectroradiometer uses three different sensors to cover the 350–2500 nm, with changeovers at 1000 nm and 1830 nm. In theory, this should have had minimal effect on the results, because all reflectance values were calibrated relative to the standard. Nevertheless, some of the individual spectra (Appendix A) showed a slight step discontinuity at 1000 nm. Furthermore, the

1830 nm changeover is spectrally coincident with an atmospheric water absorption feature, and all spectra showed strong fluctuations between 1830 nm and 1900 nm. We also noted increasing variability and amplitude in the signal from 2450 to 2500 nm that appears to be due to increased noise. As a result, no analyses at wavelengths greater than 2450 nm were undertaken.

Measurements were made in an open, outdoor area at the National Research Council of Canada's Flight Research Laboratory, Ottawa, Canada on 8 March 2011 between 13:22 and 14:22 eastern standard time under clear sky conditions. Table 1 provides the relevant atmospheric conditions and solar zenith angles during the time of data acquisition. The pelts were laid-out on a protective plastic sheet set atop an area of snow covered flat ground. Examples of how the pelts for each species were laid-out and used in this study are shown in Figure 1.

Table 1. Atmospheric and Solar Zenith information for Ottawa, ON. Canada on 8 March 2011 during the time of data acquisition. * Data from Environment Canada; † Data from National Oceanic and Atmospheric Administration.

Time (Local)	Air Temp.* (°C)	Dew Point * (°C)	Relative Humidity * (%)	Visibility * (Km)	Solar Zenith † (°)
13:22	−5.4	−17.8	37	24.1	52.5
14:22	−4.1	−18.1	33	24.1	56.6

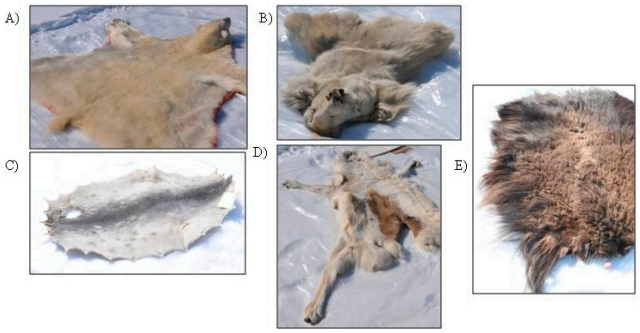

Figure 1. Examples of arctic mammal pelts used in this study: adult polar bear (**A**); juvenile polar bear (**B**); ringed seal (**C**); caribou (**D**) and muskox (**E**).

We analyzed 17 pelts from six arctic species: polar bear (*Ursus maritimus*); ringed (*Pusa hispida*), harp (*Pagophilus groenlandicus*) and bearded (*Erignatus barbatus*) seals; caribou (*Rangifer tarandus*); and muskox (*Ovibus moschatus*). Multiple measurements were taken for each pelt, to capture, in part, the variation in color pattern across each pelt (Table 2, Appendix A). The majority of samples were taken towards the middle of each pelt, to avoid any edge effects. For most pelts, this corresponds to the areas of the animal that would be most visible in an airborne/satellite survey such as along the back, neck and hindquarters. However, the juvenile polar bear pelt had been prepared by cutting it along the middle of the back with the result that the underside was sampled somewhat more heavily.

For analysis, the average spectral reflectance of each pelt was estimated by first calculating the spectral reflectance of each sample point, and then averaging the reflectance values for each spectral band equally across all samples for that pelt. This was done to simulate remotely sensed data, which typically have lower resolution sampling that provides an average reflectance across the pelt. For snow and for each pelt, we then calculated the average slope of the relationship between reflectance and wavelength separately within the UVA, the VIS, the NIR and the SWIR. Slope was calculated based on the reflectance values of the end points in each spectral range. Since the shapes of the reflectance spectra were often curvi-linear, we also calculated a novel "curvature of spectrum" measure. The curvature of spectrum is the mean of the distance (in measured units *i.e.*, % reflectance) of each measured spectral point value from the line connecting the reflectance at the end points of the spectral range. If the average is negative then the spectrum is predominantly concave in that interval; if positive

it is predominantly convex. Increased absolute values of the average deviation indicate increased curvature (concave or convex) of the spectral segment.

Table 2. Number of spectral samples taken from each pelt analyzed.

Mammal Species	Pelt #	Age	# of Samples
Ringed Seal, *Pusa hispida*	1	Adult	3
	2	Adult	2
	3	Juvenile	2
	4	Adult	3
	5	Adult	3
	6	Adult	3
	7	Adult	3
	8	Adult	3
Harp Seal, *Pagophilus groenlandicus*	1	Adult	6
Bearded Seal, *Erignatus barbatus*	1	Adult	4
Caribou *Rangifer tarandus*	1	Adult	5
	2	Adult	9
	3	Adult	6
Musk-Ox, *Ovibos moschatus*	1	Adult	8
Polar Bear, *Ursus maritimus*	1	Juvenile	4
	2	Adult	7
	3	Adult	10

To quantify the difference between the average spectrum for each pelt with the average spectrum of snow, as well as between the spectra of polar bear pelts and those of the other pelts, we used the spectral shape metric (θ). The θ metric describes differences in the angle between spectra [29] and is calculated based on Equation (1):

$$\theta = \boldsymbol{cos}^{-1}\left[\frac{\int \boldsymbol{S}_1(\lambda)\,\boldsymbol{S}_2(\lambda)\,\delta\lambda}{[\int \boldsymbol{S}_1(\lambda)^2\,\delta\lambda]^{\frac{1}{2}}[\int \boldsymbol{S}_2(\lambda)^2\,\delta\lambda]^{\frac{1}{2}}}\right] \quad (1)$$

where $S_1(\lambda)$ and $S_2(\lambda)$ represent the spectral values of each spectrum being compared at wavelength λ. These are integrated over the range of λ values being considered in each analysis. For the full data set (ASD), the spectral range was 350–2500 nm with 1 nm resolution. To estimate the potential discrimination based on various existing satellite sensors, we also repeated the calculations using the average reflectance in each of the spectral bands for the Pleiades, WorldView-2 and WorldView-3 satellites [30]. Figure 2 illustrates the coverage of each band per satellite in the reflective electromagnetic spectrum. These resulting calculated spectra were simulated from the ASD spectra using the spectral response functions for each satellite sensor in ENVI 5.1. For WorldView-3, the pixel sizes differ for the Visible and NIR (1.24 m) and the SWIR (3.7 m) so we analyzed them separately.

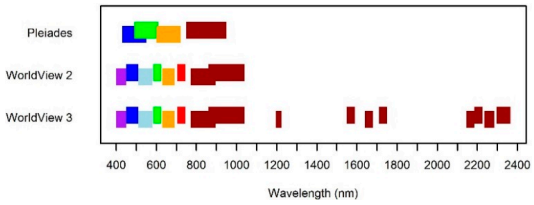

Figure 2. Spectral band placement and widths (in nm) within the reflective portion of the electromagnetic spectrum for: Pleiades (430–550, 490–610, 600–720, 750–950), WorldView-2 (400–450, 450–510, 510–580, 585–625, 630–690, 705–745, 770–895, 860–1040) and WorldView-3 (400–450, 450–510, 510–580, 585–625, 630–690, 705–745, 770–895, 860–1040, 1195–1225, 1550–1590, 1640–1680, 1710–1750, 2145–2185, 2185–2225, 2235–2285, 2295–2365).

3. Results and Discussion

3.1. Results

All of the mammal pelts could be readily distinguished from snow by a combination of low reflectance in the UVA for the pelts and higher reflectance in the NIR and SWIR (Figures 3–5). Most pelts averaged <10% at 350 nm, including all the bears (Figure 3), with variation among individuals ranging from nearly 0% reflectance for some of the seals and the Muskox (Figures 4 and 5) up to slightly above 15% in two of the caribou (Figure 5). For all species, reflectance then increased to peak in the SWIR around 1300 nm. Peak reflectance varied from 40% to 80% depending on the pelt. Reflectance then dropped at longer wavelengths, but still remained at least half of the peak reflectance up to 1800 nm and, in most pelts, up to 2450 nm. In contrast, reflectance from snow was highest in the UVA, exceeding 90% at 350 nm (Figures 3–5). It declined gradually through the visible range reaching about 80% at the NIR, and then further declined rapidly to approach 0% at 1500 nm, which is known to be a large absorption band for water. At longer wavelengths, reflectance varied, showing small peaks at around 1850 nm and 2250 nm, with lows at 2000 nm (attributed to water and CO_2 absorption) and 2450 nm.

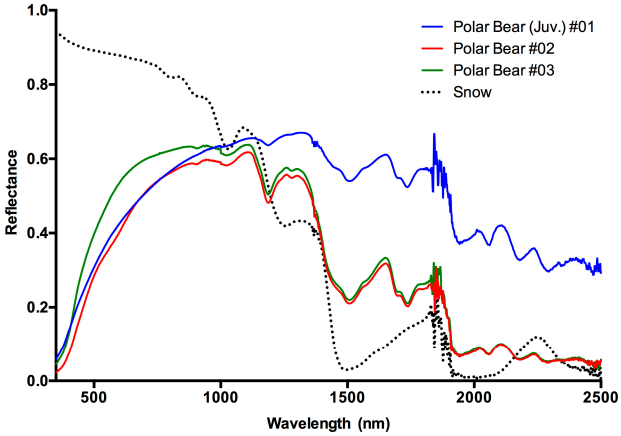

Figure 3. Average spectral reflectance of two adult (red and green lines) and one juvenile polar bear pelts (blue line) in relation to that of clean snow (dashed line) showing the very low reflectance in the UVA, increasing reflectance in the visible, and high reflectance in the infrared, in relation to snow.

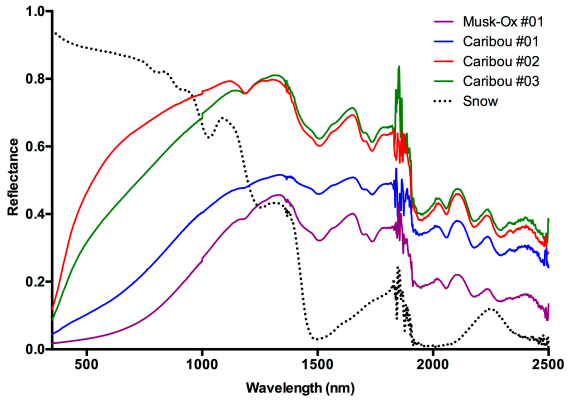

Figure 4. Average spectral reflectance of three adult caribou pelts (blue, red and green lines), and one muskox pelt (violet line) in relation to that of clean snow (dashed line). All pelts had low reflectance in the UVA. The two caribou pelts with the highest reflectance were very pale individuals, appearing nearly white to the human eye in the visible range, but all skins showed relatively high reflectance in the near infrared.

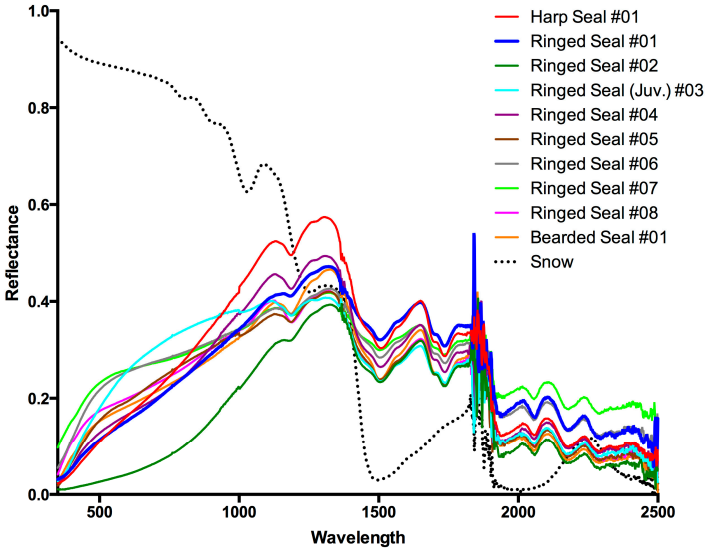

Figure 5. Average spectral reflectance of 10 pelts of three different seal species–ringed, harp and bearded—in relation to that of clean white snow (dashed line). As with the other arctic mammals of this study, all seal species have low reflectance in the UVA compared to snow. Despite conspicuous differences in color patterns, the average reflectance values were similar for seals of all three species.

While all mammals could be distinguished from snow within the VIS region, the greatest contrast was achieved by comparing the pelts to snow in the UVA region, where reflectance of snow was much higher than that of mammals. Within the NIR region, the difference between the snow and pelts' reflectance values decreased to zero towards 1000 nm for the polar bears and the lighter caribou, and remained similar up to about 1200 nm. Above 1400 nm, all mammals reflected much more strongly than snow.

The shape and trend of the reflectance curve for each mammal, as well as for the snow, varied considerably for the entire 350–2450 nm range. Calculation of the slope (Table 3) and curvature parameters (Table 4) within the UVA, VIS, NIR and SWIR regions provide a basic analysis of the reflectance curve.

Table 3. Slope of average reflectance against wavelength in various spectral regions based upon the average reflectance spectra from snow and from each mammal pelt.

Sample Material	n	Slope of Average Spectra (% Reflectance/nm)			
		UVA (350–400 nm)	**VIS (400–770 nm)**	**NIR (770–1000 nm)**	**SWIR (1000–2450 nm)**
Snow	10	−0.06 (±0.01)	−0.02 (±0.00)	−0.07 (±0.00)	−0.04 (±0.00)
Polar bear (Adult)	2	0.13 (±0.03)	0.15 (±0.01)	0.01 (±0.01)	−0.04 (±0.01)
Polar bear (Juv.)	1	0.15	0.12	0.04	−0.02
Caribou	3	0.16 (±0.1)	0.09 (±0.01)	0.06 (±0.01)	−0.02 (±0.01)
Muskox	1	0.01	0.02	0.07	−0.01
Ringed Seal	8	0.08 (±0.02)	0.05 (±0.02)	0.04 (±0.01)	−0.02 (±0.00)
Bearded seal	1	0.10	0.04	0.04	−0.02
Harp seal	1	0.04	0.06	0.07	−0.02

Table 4. Degree of curvature of the average reflectance spectrum of each skin in each spectral region.

Sample Material	Curvature of Spectrum (% Reflectance/nm)											
	UVA (350–400 nm)			VIS (400–700 nm)			NIR (700–1000 nm)			SWIR(1000–2450 nm)		
	Average Deviation %	Largest Deviation		Average Deviation %	Largest Deviation		Average Deviation %	Largest Deviation		Average Deviation %	Largest Deviation	
		%	nm		%	Nm		%	nm		%	Nm
Snow	−0.1	−0.1	380	−0.3	0.0	684	3.3	6.0	950	−14.0	−42.0	1484
Polar Bear #1 (Juvenile)	−0.8	−1.4	380	7.9	11.6	518	1.3	2.1	865	3.7	12.7	1654
Polar Bear #2	−0.5	−0.9	377	3.4	5.3	550	1.3	1.3	855	−5.3	−18.9	1502
Polar Bear #3	−0.6	−1.0	387	3.9	6.8	518	3.4	3.4	947	−6.5	−20.5	1503
Caribou #1	−0.1	−0.1	374	−0.5	−1.0	596	0.1	0.7	942	7.2	15.9	1655
Caribou #2	−0.5	−0.8	376	5.4	8.0	516	0.8	1.2	857	3.2	13.6	1331
Caribou #3	−0.2	−0.3	377	2.5	4.0	503	0.6	1.0	890	6.7	20.2	1332
Musk-Ox	−0.0	−0.1	364	−0.6	−1.0	579	−1.2	−1.9	823	9.3	22.5	1338
Ringed Seal #1	−0.2	−0.4	380	0.7	1.3	487	−0.1	−0.3	941	6.6	18.3	1329
Ringed Seal # 2	−0.1	−0.2	372	−0.4	−0.6	585	−1.3	−2.1	846	7.3	21.0	1335
Ringed Seal #3 (Juvenile)	−0.4	−0.7	380	2.4	3.5	566	0.7	1.0	853	0.0	9.0–9.0	1330 1935
Ringed Seal # 4	−0.3	−0.5	375	1.5	2.4	502	−1.0	−1.7	834	3.0	17.8	1324
Ringed Seal # 5	−0.3	−0.6	371	1.8	3.2	518	0.3	0.6	934	−0.5	10.7	1331
Ringed Seal # 6	−0.2	−0.3	381	3.1	5.0	517	−0.2	−0.4	814	3.7	13.5	1333
Ringed Seal # 7	0.2	0.3	367	2.4	3.9	517	−0.4	−0.8	817	5.7	12.7	1329
Ringed Seal # 8	0.2	0.3	389	1.4	2.6	488	0.0	0.7	946	2.7	14.3	1328
Bearded Seal #1	−0.0	−0.2	361	1.7	3.0	489	−0.3	−0.5	830	4.8	20.2	1329
Harp Seal #1	−0.2	−0.3	376	0.5	0.9	518	−0.4	−0.7	814	4.5	22.5	1319

Within the UVA, the slope of the snow reflectance pattern had a negative value (−0.06% reflectance; Table 3), indicating a decreasing reflectance with increasing wavelength, with little deviation from a straight line (maximum deviation of −0.1% reflectance; Table 4). In contrast, within the UVA region, all mammal pelts had a positive slope varying from very small values (0.01% reflectance for Musk-Ox) to very large (0.16% reflectance for Caribou; Table 3). Again, there was relatively little curvature, although most pelts showed a slightly concave curve (negative values) with only two ringed seal pelts having slightly convex curves (Table 4).

Within the VIS wavelength region, snow still showed a negative slope (−0.02% reflectance), albeit less than in the UVA region, while all mammals had a positive slope varying from 0.02% reflectance to 0.15% reflectance (Table 3). In this region, adult polar bears had the highest slope, while the juvenile polar bear and the caribou had similar slopes, reflecting the similar spectra of the two (Figures 3 and 4). The average slopes of the seals were lower in this region compared to the UVA region (Table 3). However, the Musk-Ox spectral slope doubled in comparison to the UVA region. Nearly all spectra were much less linear in this region, with most having strongly convex curves (positive deviations); although the Musk-Ox, one Caribou and one seal had concave curves (Table 4).

Within the NIR, the slope of the snow spectra was still negative, although less strongly so (−0.07% reflectance/nm), while those of most mammals produced similar results that were slightly positive (Table 3). In this region, the slope of the polar bears changed the most from 0.15 (±0.01) % reflectance/nm in the VIS to 0.01 (±0.01) % Reflectance/nm in the NIR. Most spectra were only slightly curved in this region with similar numbers slightly convex (positive) or slightly concave (Table 4).

Within the SWIR, the snow spectrum had a negative slope (−0.04% reflectance/nm) indicating that the amplitude of the reflectance was strongly reduced with increased wavelength. In this range, all mammals also showed negative slopes, indicating reduced reflectance in the longer wavelength SWIR—from values of near 60% at 1000 nm to below 10% at 2450 nm for polar bears. However, the relationships were generally quite strongly non-linear, as shown by the curvature measures, with relatively high deviations from a straight line for both snow and most pelts (Table 4). In many cases, the curvature fluctuated from negative to positive through the range. Most of the largest deviations occurred in the range 1319–1338 nm, along a water absorption feature lobe. Note that measurements between 1800 and 1900 nm may not be reliable, as they correspond to both a changeover in the sensor (at 1830 nm) as well as some complex water absorption features.

There was also substantial variation within species among individuals in their reflectance patterns. All three bear pelts showed similar reflectance patterns through to about 1200 nm (Figure 3). However, at longer wavelengths in the SWIR, the juvenile pelt showed much higher reflectance than the adult pelts. Among caribou, two very pale pelts had very similar reflectance patterns with convex curves through the visible and very high reflectance in the SWIR (Figure 5). In contrast, the darker pelt had much lower reflectance, with a convex shape in the visible and NIR, though its reflectance values in the SWIR approached those of the paler pelts. Most of the seals, regardless of species, had similar average reflectance curves, though one individual was markedly darker than the rest (Figure 5). Within pelts, different portions of the pelts of most species differed somewhat in intensity but had similarly shaped curves (Appendix A). However, some of the seal pelts had more strongly patterned light and dark marks on their fur, and the reflectance patterns thus varied more strongly on different parts of the pelt (Appendix A), but such variance would not be relevant to remote sensing imagery with pixel sizes that measure average reflectance over large parts of the animal.

Based on simulated reflectance patterns from a sample of currently available high spatial resolution satellite imagery (WorldView-2, WorldView-3, Pleiades), all mammal pelts had noticeably different reflectance curves than clean white snow (Figures 3–5). The difference in spectral shape was greatest for the Worldview satellites due to the broader spectral range. The VIS-NIR and SWIR ranges for the WorldView-3 satellite were considered separately due to their different spatial resolutions (1.2 and 3.7 m, respectively). Quantitative analyses based on the θ metric confirm that all pelts can be distinguished from snow (Figure 6). Dissimilarity between the mammals and snow was strongest

based on the full ASD spectral range (350–2450 nm), although it was only marginally less based on the combined range of WorldView-3. However, it is important to remember that the spatial resolution of the two sensors from WorldView-3 (VIS-NIR and SWIR) result in different spatial resolutions, therefore, combining the spectra from the two data sets from an actual image so that the spectra continuously spans the entire data range over some exact surface location is not possible as the resulting spectra from each pixel would be the summation from different fields of view. The θ values were lowest for the WorldView-3 SWIR range (Figure 7e), Pleiades (Figure 7b) and WorldView-2 (Figure 7c) satellites, as might be expected due to the more limited bandwidth and, in the case of Pleiades, fewer individual bands.

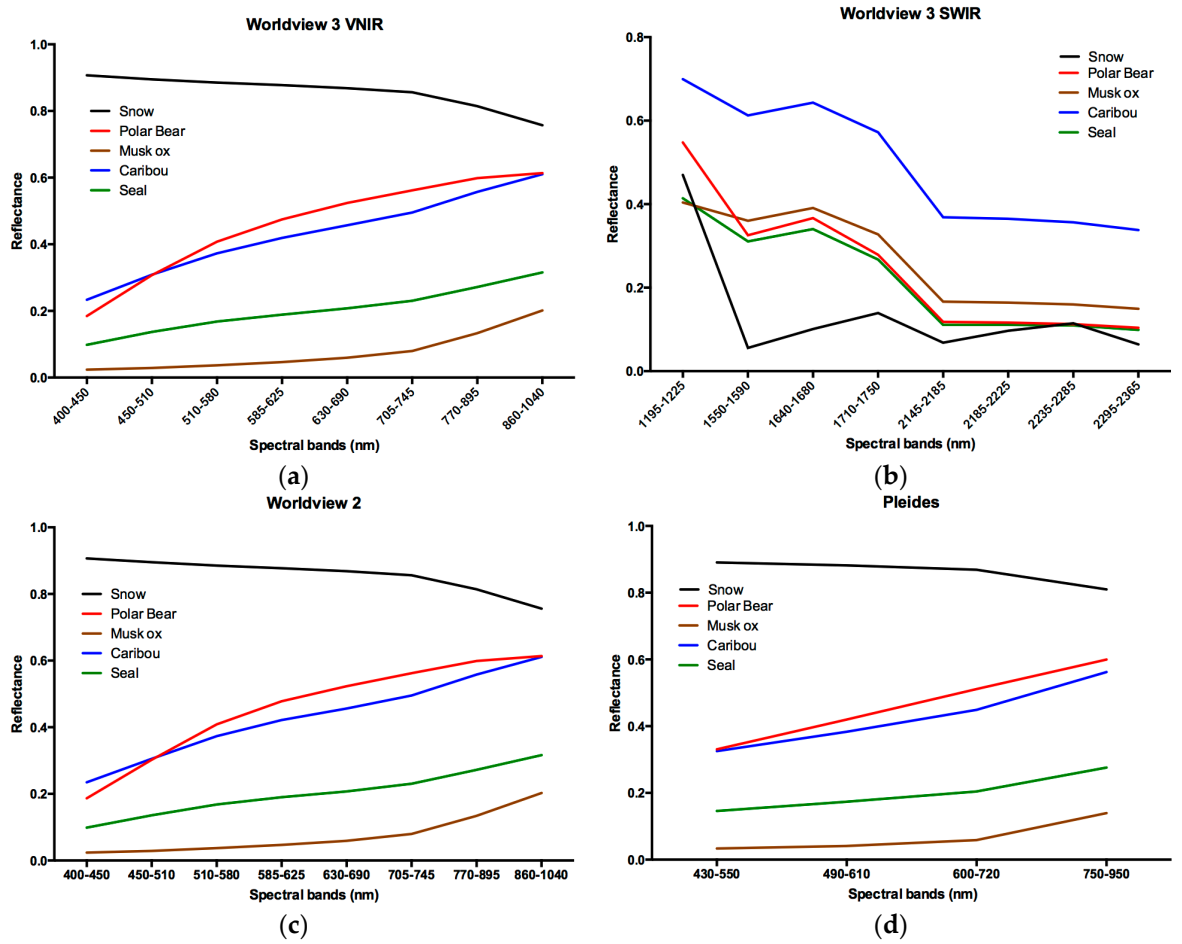

Figure 6. Simulation of spectral reflectance patterns for four different satellite configurations: (**a**) WorldView-3 VIS to NIR (8-band multispectral); (**b**) WorldView-3 SWIR (8-band multispectral); (**c**) WorldView-2 (8-band multispectral); (**d**) Pleiades (4-band multispectral).

There was greater dissimilarity between the reflectance of the different mammal species in comparison to the spectrum of an adult polar bear than among the spectra of the different polar bear skins, based on the θ metric (Figure 7) indicating the variability within the polar bears is low. Considering only the visible and NIR, all the bears had low variation compared to differences with other species. The muskox was the most distinctly different from the polar bear, as long as the visible and NIR bandwidths were included in the analysis. Other species differed, on average, from polar bears, especially if the full spectral range was available, though there was considerable individual variation, and some species could potentially be confounded with polar bears with the limited spectral resolution of the satellite sensors.

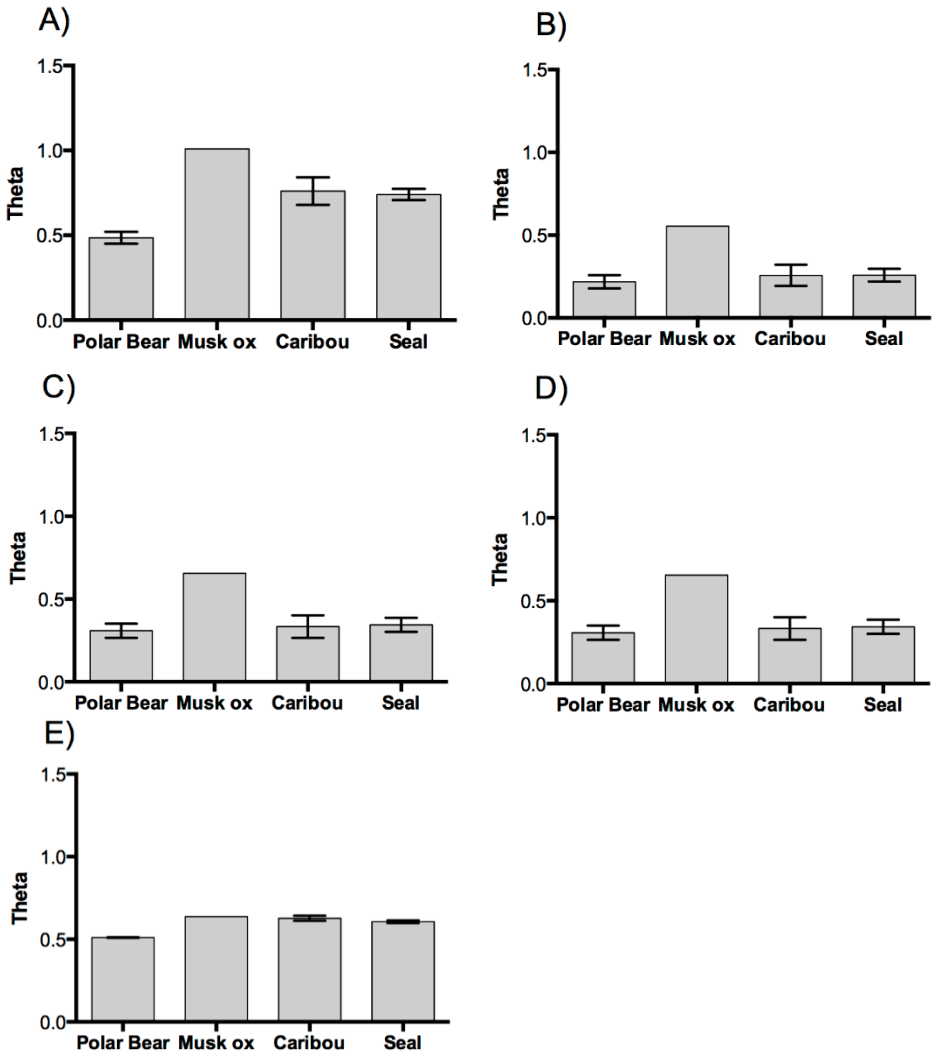

Figure 7. Dissimilarity in spectral shape (θ metric) of the mammal pelts *versus* clean snow for the full range ASD spectroradiometer data (**A**) and based on simulated data of spectral reflectance patterns for four different satellite configurations: (**B**) Pleiades (4-band multispectral); (**C**) WorldView-2 (8-band multispectral); (**D**) WorldView-3 VIS to NIR (8-band multispectral); (**E**) WorldView-3 SWIR (8-band multispectral). Larger values of θ indicate greater dissimilarity between the mammal and snow spectra.

3.2. Discussion

Our results indicate that all of the mammal species we considered can be very easily differentiated from clean snow based on a combination of very low reflectance in the UVA and high reflectance in the SWIR (Figures 3–6). Even within the visible range and NIR bands that are available from satellites, all species could be differentiated from snow based on increasing reflectance from short to long wavelengths in the mammals, in contrast to a slight decrease in reflectance in the same range of snow (Figures 3–6).

These reflectance patterns for bears are qualitatively similar to those reported by previous studies. Lavigne and Øritsland (1974) [19,20] showed that polar bears appear as black against a white snow background when photographed in the UVA. They used Kodak Double-X Aerographic Film 2405, which is an emulsion-based film that is sensitive within the 250–700 nm range [31], combined with a Kodak 18A filter that only transmits light at 300–400 nm and 700–900 nm; the combination would thus be sensitive only to the 300–400 nm range, overlapping the range we sampled (350–400 nm). Those authors similarly found high absorption in the UVA of seal pelts, though they found relatively higher

reflectance values for an Arctic hare (*Lepus arcticus*) pelt, a species we did not measure. Grojean *et al.*, (1980) [22] published a spectral reflectance curve for a polar bear pelt from the UVA to NIR, which had a similar shape to ours, though with somewhat higher overall reflectance. It is not clear whether the higher reflectance represents variation among pelts, or differences in measurement equipment.

We also found that pelts of polar bears could be differentiated from most other pelts, provided the full spectral band width is available (Figure 8). Muskox was the most distinctly different, with very dark fur that had especially low reflectance in the blue end of the visible range, although it was more similar to bears in the SWIR (Figure 4). Two of the palest caribou pelts had very similar reflectance patterns to the juvenile polar bear, though their reflectance in the SWIR was much higher than that of the adult polar bears. Measurement of additional animals would be useful to test the consistency of these differences.

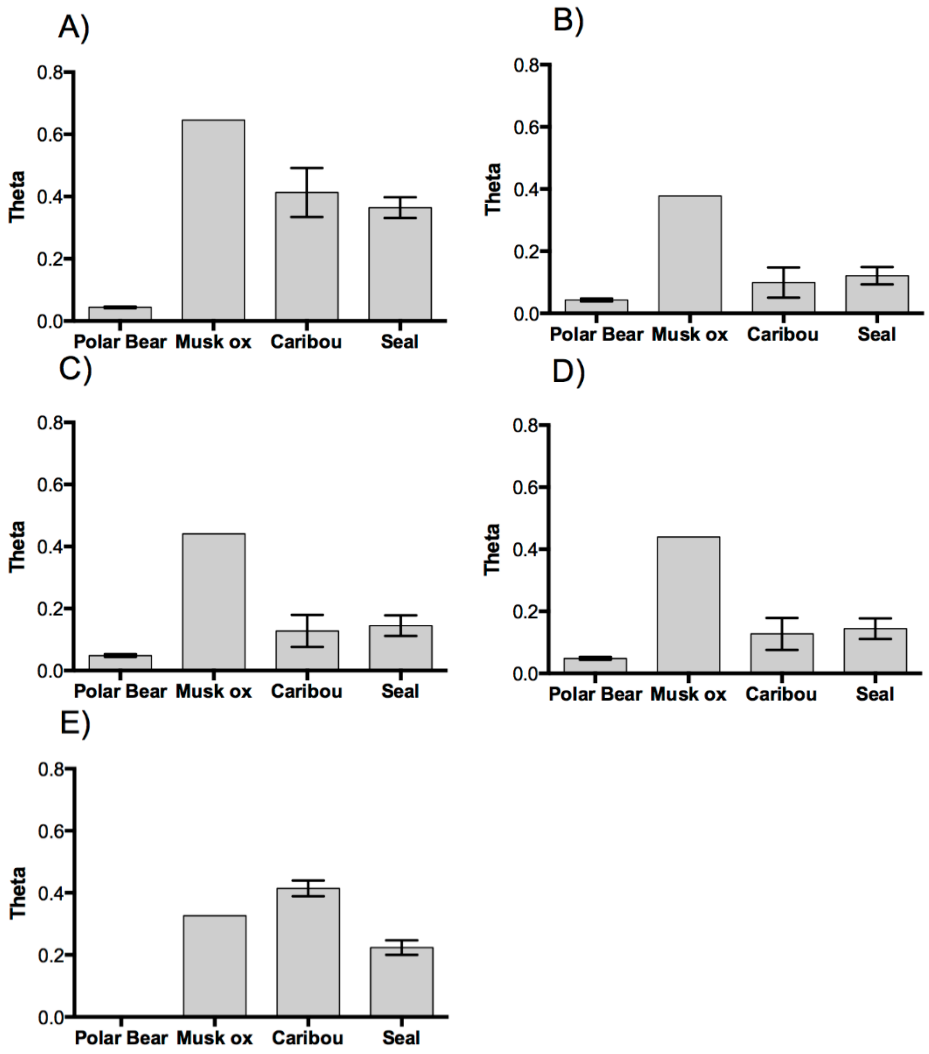

Figure 8. Dissimilarity in spectral shape (θ metric) of the mammal pelts *versus* the average spectrum of the adult polar bear for the full range ASD spectroradiometer data (**A**) and based on simulated data of spectral reflectance patterns for four different satellite configurations: (**B**) Pleiades (4-band multispectral); (**C**) WorldView-2 (8-band multispectral); (**D**) WorldView-3 VIS to NIR (8-band multispectral); (**E**) WorldView-3 SWIR (8-band multispectral). Larger values of θ indicate greater dissimilarity between the mammal and snow spectra.

The applicability of these results to remote sensing surveys depends on a number of factors including the similarity of our pelt measurements to those of live animals, the spectral reflectance

patterns of the background and other environmental contaminants, and the availability of appropriate sensors. All of our measurements were based on museum pelts, which could potentially differ from live animals for several reasons. The process of preserving and tanning pelts can affect the color and thus the reflectance patterns of fur [32]. Similarly, fur color in museum specimens can change over time [33]. The time of year of collection could also affect fur color with, for example, freshly molted polar bear fur tending to appear whiter and less yellowish [34]. Unfortunately, most of the pelts loaned to us for this project were lacking collection data, so we do not have information on the time of year they were collected, how long ago they were collected, or how they were treated during preservation. The observed differences in reflectance in the infrared between the juvenile and adult polar bear pelts (Figure 3) could potentially be due to differences in freshness, wear or treatment of the fur, rather than age differences *per se*. Nevertheless, most reported impacts of preservatives or aging on color of mammal pelts relate to reddening of dark colors ("foxing"), which would not affect polar bears [32,33]. Although white colors could obviously become stained, the general color and pattern of all of the pelts, at least in the visual range, appeared to fit within the range of variation observed in live animals, although the polar bear pelts were darker than some, and some of the seal pelts appeared to be slightly foxed or stained with oils. We are not aware of any studies examining the impacts of preservation on reflectance of mammal pelts outside of the visual range.

Differentiating mammals in remote sensing imagery depends also on the background. Our work was primarily motivated by trying to detect bears when they are against a snow/ice background. Gerland *et al.*, (1999) [35] reported reflectance patterns for sea ice that were very similar to those we found for clean white snow suggesting that the same patterns we observed could differentiate bears and other mammals from sea ice. Nevertheless, a variety of confounding factors could complicate automated detection. Although few objects other than animals or human structures are likely to be found on sea ice, patches of open water and areas of water above snow, whether caused by melt or by seepage, they could have very different reflectance patterns from clean snow. Furthermore, various contaminants could affect snow color, including blood stains where bears have killed seals or other prey. Pressure ridges and other irregularities would produce extensive, irregular shadows.

Any analysis would also have to consider the changing spectral patterns of incident light associated with changing sun angles. Thus, although we found that all species could be readily differentiated from clean white snow in any of the UVA, visual, NIR or SWIR wavebands, a combination of wavelengths may be necessary to reduce the risk of false positives—*i.e.*, detection of areas of ice or water with similar spectral properties to mammals.

The ability to detect polar bears and other animals depends also on the type of imaging equipment available. Using existing satellite imagery, our analyses indicate that we can more readily differentiate mammals using the visible to NIR wavelengths available from WorldView-2 or 3, compared to the more limited spectral bands of Pleiades (Figure 7). Discrimination can potentially be further improved with the SWIR from WorldView-3; however, that imagery is only available at a relatively coarse pixel size (3.7 m), which is much larger than the size of any of these mammals, and, hence, would have a greatly diluted signal. Even the visible to NIR bands with WorldView-3 only have a resolution of 1.2 m. Thus, the animal would only be present in 1 or a few pixels, each of which would overlap to some degree with the background, thus reducing the distinctiveness of the signal. The panchromatic imagery has a resolution of 0.31 m, which would allow 10–30 pixels per animal for larger mammals like caribou or bears. Pan sharpening the multispectral imagery would improve resolution, but could blur some of the spectral distinctions. Even 10–30 pixels per animal would not be enough detail to confirm the identifications visually based on shape. Airborne UVA/VIS/NIR/SWIR camera systems could also be used. One option would be to use moderate resolution multi-spectral imagery (e.g., 0.5–1.0 m pixels) to detect potential bears based on the spectral signature, combined with higher resolution (e.g., 0.1 m) standard photographs to verify species identification visually, using techniques analogous to those of [13].

The cost effectiveness and efficiency of different options and the need for visual verification will depend strongly on the specificity and discrimination of the spectral signatures.

4. Conclusions

This work has measured the spectroscopic signature of snow and several arctic mammal pelts under winter conditions. Arctic species measured were: polar bear adults, polar bear juvenile, caribou, musk-ox, ringed seal, harp seal and bearded seal. The work has extended the spectral coverage and increased the spectral resolution of the spectral reflectance curves for the measured animal pelts. Where spectral overlap exists with previous studies, this study is in agreement with those data.

A basic analysis of potential spectral detection and differentiation between snow and polar bears (and the other arctic mammal pelts) by current space borne optical satellites, (Pleiades, WorldView-2 and 3) show that it may be possible. However, no attempt at a rigorous assessment of space borne spatial analysis has been undertaken in this work. The work here was fully conducted within the spectral domain.

Further field testing imaging live animals is needed to verify the spectral signatures detected in our study, and to determine the minimum number of bands that need to be analyzed to reliably detect bears and other animals while minimizing the number of false positives from other objects in the environment.

Acknowledgments: The authors would like to thank the Canadian Museum of Nature for the loan of the pelts used in this study, especially Kamal Khidas who arranged permissions, and Marcie Kwindt who helped in the field.

Author Contributions: G.L. and C.F. conceived the study; G.L., C.F., R.S. collected and processed the data; G.L., C.F., M.K., J.G. analyzed the data. All authors contributed to the writing and editing of the manuscript.

Conflicts of Interest: The authors declare no conflict of interest.

Appendix A

Source data used to calculate spectral averages for each mammal pelt.

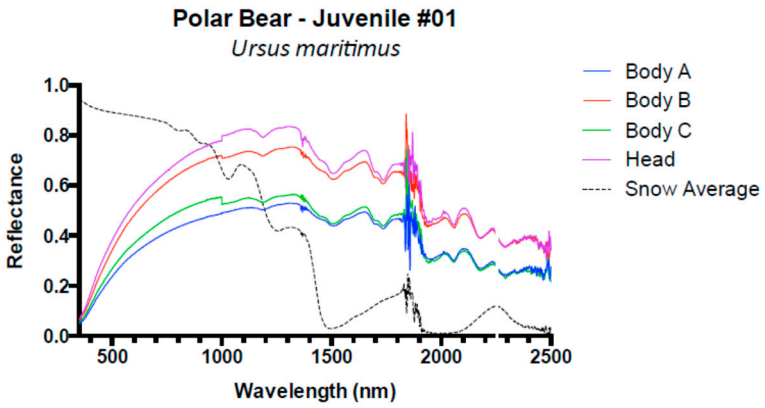

Figure A1. Spectral reflectance measurement of snow average along with measurements of various locations from the pelt 01 Juvenile Polar Bear. These data were used to calculate an average spectral reflectance for the pelt.

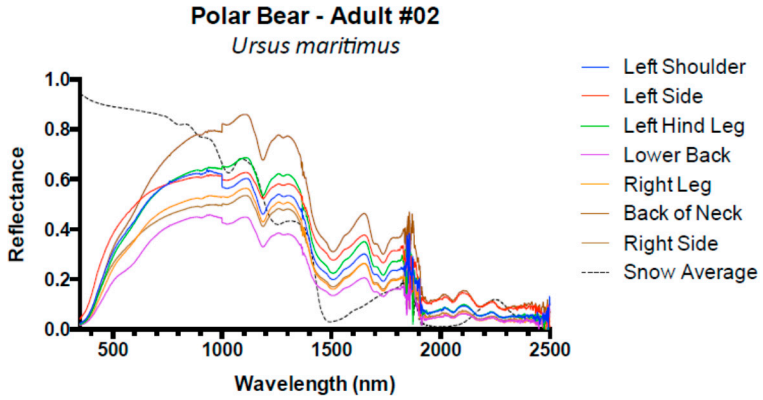

Figure A2. Spectral reflectance measurement of snow average along with measurements of various locations from the pelt 02 Adult Polar Bear. These data were used to calculate an average spectral reflectance for the pelt.

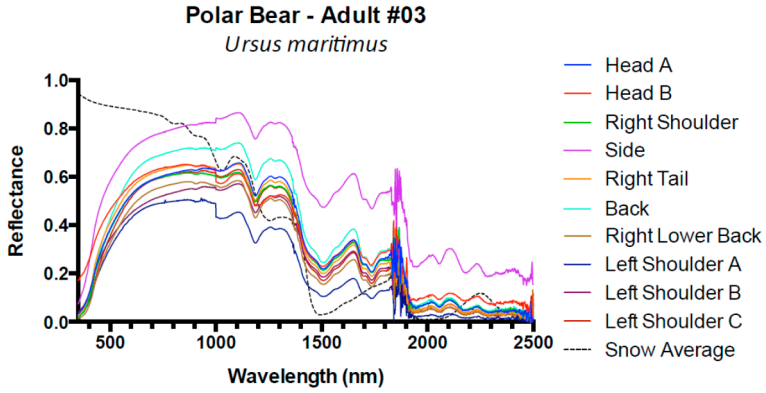

Figure A3. Spectral reflectance measurement of snow average along with measurements of various locations from the pelt 03 Adult Polar Bear. These data were used to calculate an average spectral reflectance for the pelt.

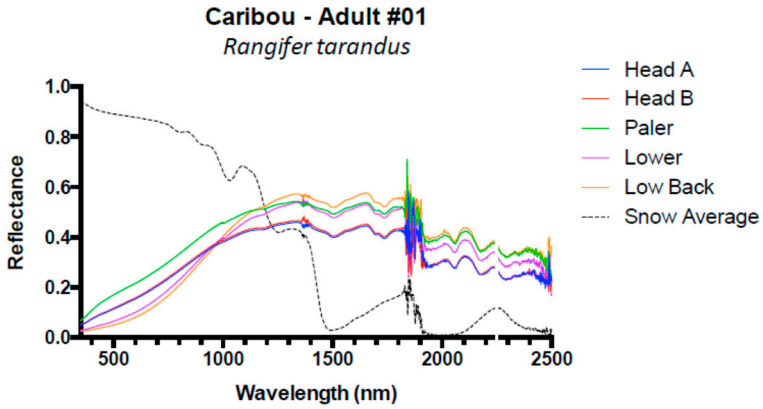

Figure A4. Spectral reflectance measurement of snow average along with measurements of various locations from the pelt 01 Adult Caribou. These data were used to calculate an average spectral reflectance for the pelt.

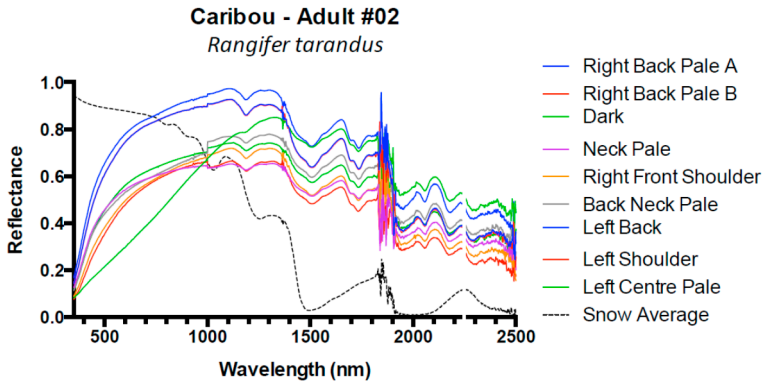

Figure A5. Spectral reflectance measurement of snow average along with measurements of various locations from the pelt 02 Adult Caribou. These data were used to calculate an average spectral reflectance for the pelt.

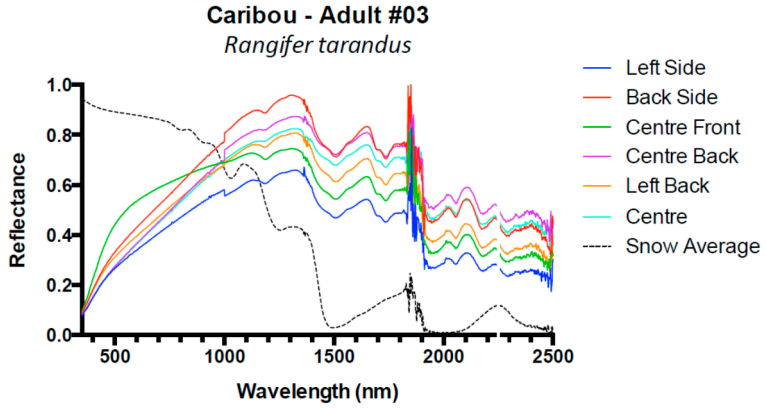

Figure A6. Spectral reflectance measurement of snow average along with measurements of various locations from the pelt 03 Adult Caribou. These data were used to calculate an average spectral reflectance for the pelt.

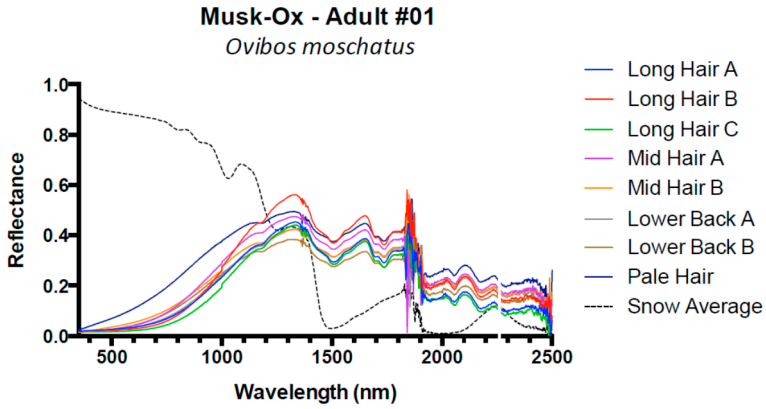

Figure A7. Spectral reflectance measurement of snow average along with measurements of various locations from the pelt 01 Adult Musk-Ox. These data were used to calculate an average spectral reflectance for the pelt.

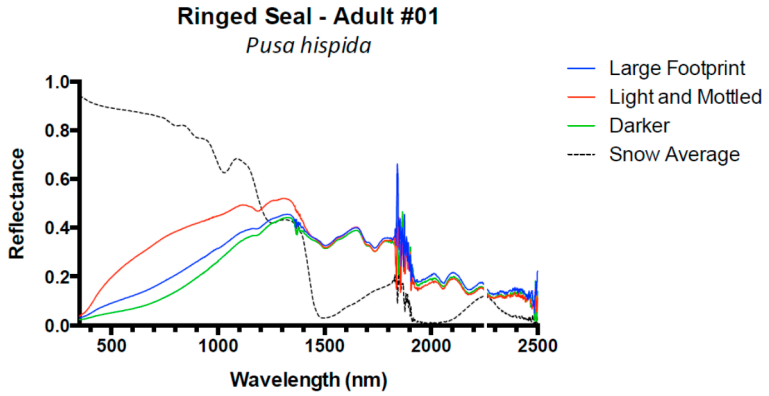

Figure A8. Spectral reflectance measurement of snow average along with measurements of various locations from the pelt 01 Adult Ringed Seal. These data were used to calculate an average spectral reflectance for the pelt.

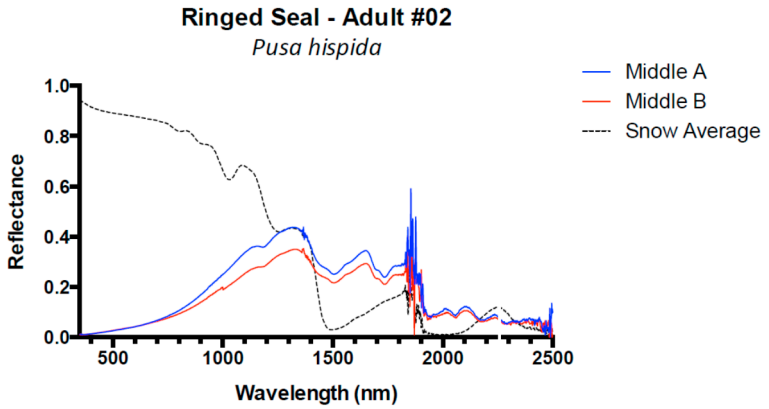

Figure A9. Spectral reflectance measurement of snow average along with measurements of various locations from the pelt 02 Adult Ringed Seal. These data were used to calculate an average spectral reflectance for the pelt.

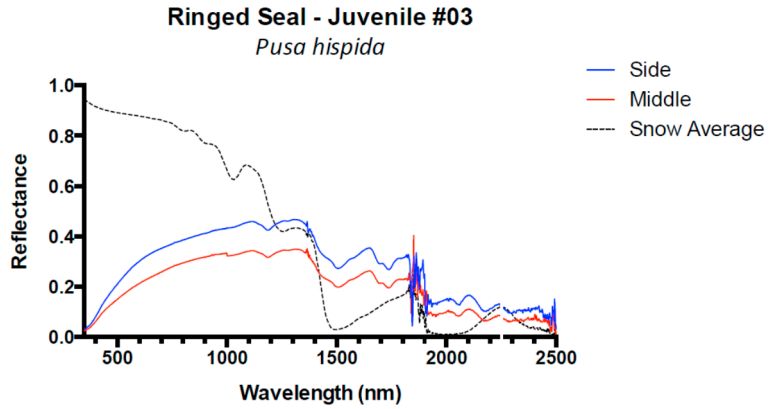

Figure A10. Spectral reflectance measurement of snow average along with measurements of various locations from the pelt 03 Juvenile Ringed Seal. These data were used to calculate an average spectral reflectance for the pelt.

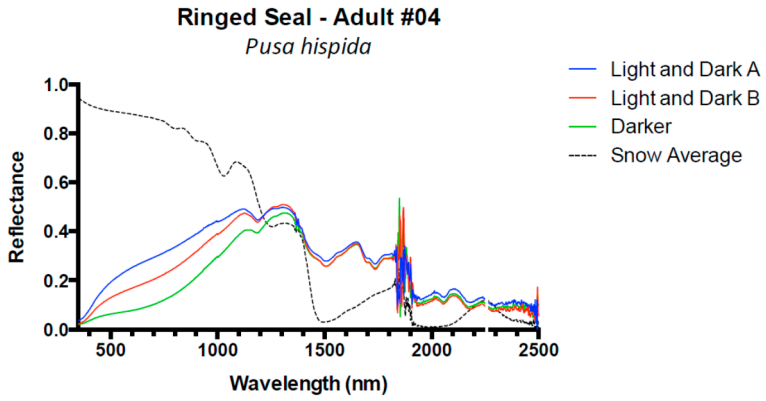

Figure A11. Spectral reflectance measurement of snow average along with measurements of various locations from the pelt 03 Adult Ringed Seal. These data were used to calculate an average spectral reflectance for the pelt.

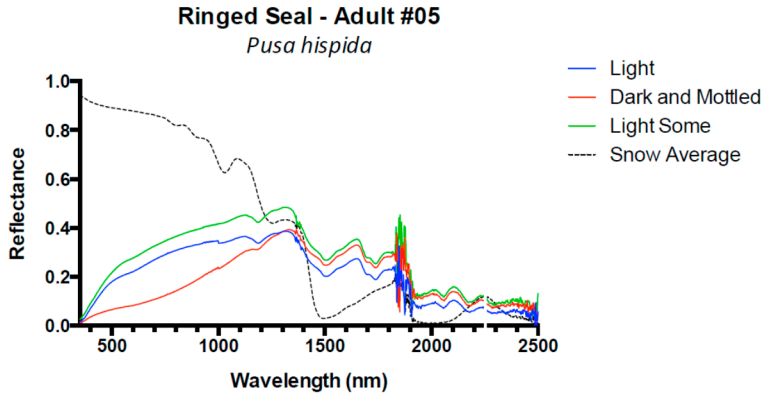

Figure A12. Spectral reflectance measurement of snow average along with measurements of various locations from the pelt 04 Adult Ringed Seal. These data were used to calculate an average spectral reflectance for the pelt.

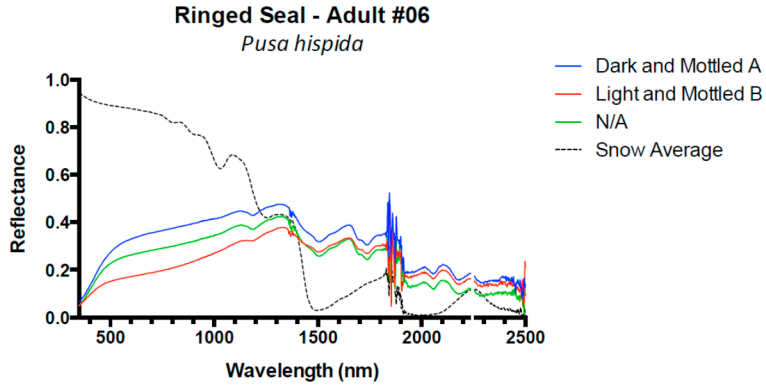

Figure A13. Spectral reflectance measurement of snow average along with measurements of various locations from the pelt 06 Adult Ringed Seal. These data were used to calculate an average spectral reflectance for the pelt.

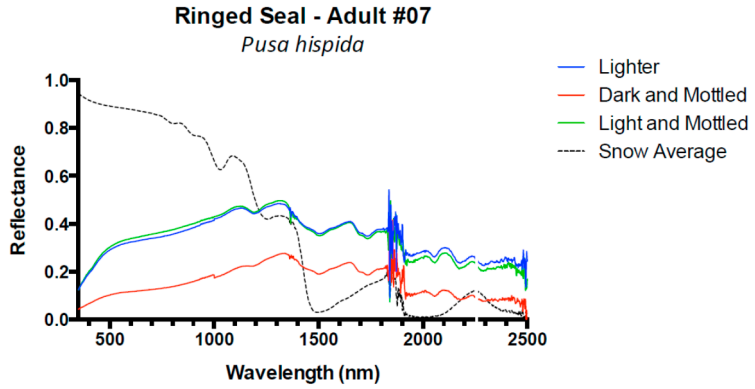

Figure A14. Spectral reflectance measurement of snow average along with measurements of various locations from the pelt 07 Adult Ringed Seal. These data were used to calculate an average spectral reflectance for the pelt.

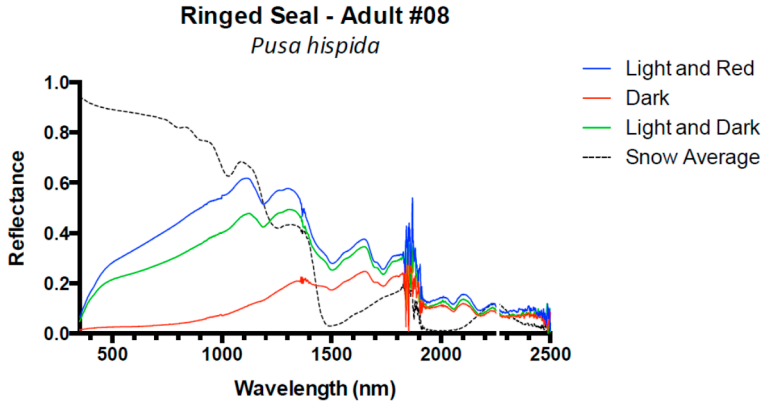

Figure A15. Spectral reflectance measurement of snow average along with measurements of various locations from the pelt 08 Adult Ringed Seal. These data were used to calculate an average spectral reflectance for the pelt.

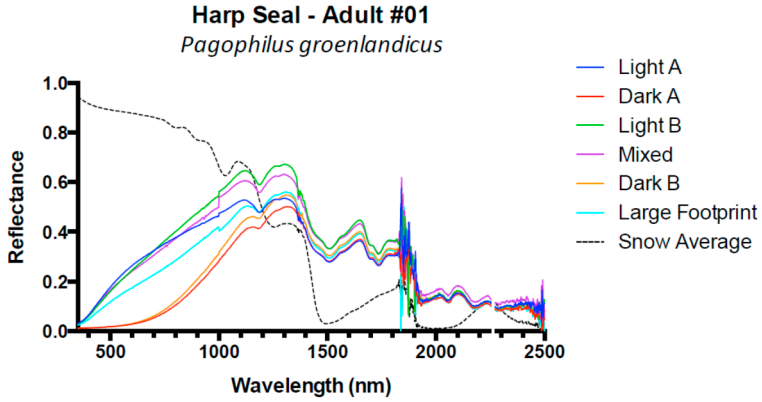

Figure A16. Spectral reflectance measurement of snow average along with measurements of various locations from the pelt 01 Adult Harp Seal. These data were used to calculate an average spectral reflectance for the pelt.

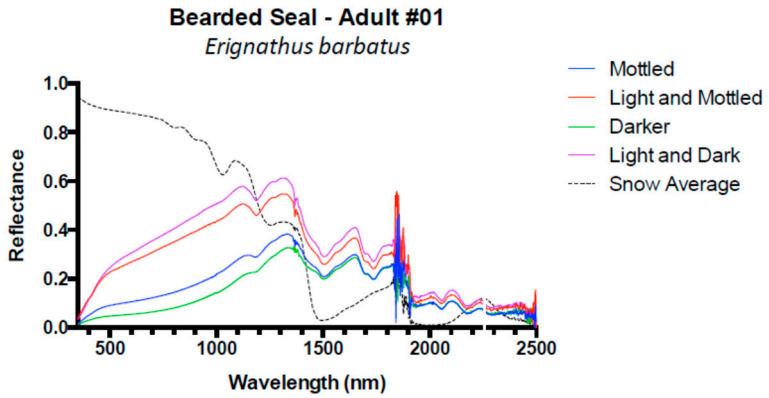

Figure A17. Spectral reflectance measurement of snow average along with measurements of various locations from the pelt 01 Adult Bearded Seal. These data were used to calculate an average spectral reflectance for the pelt.

References

1. Comiso, J.C.; Parkinson, C.L.; Gersten, R.; Stock, L. Accelerated decline in the Arctic Sea ice cover. *Geophys. Res. Lett.* **2008**, *35*. [CrossRef]
2. Regehr, E.V.; Lunn, N.J.; Amstrup, S.C.; Stirling, L. Effects of earlier sea ice breakup on survival and population size of polar bears in western Hudson bay. *J. Wildl. Manag.* **2007**, *71*, 2673–2683. [CrossRef]
3. Stirling, I.; Parkinson, C.L. Possible effects of climate warming on selected populations of polar bears (*Ursus maritimus*) in the Canadian arctic. *Arctic* **2006**, *59*, 261–275. [CrossRef]
4. Stirling, I.; Lunn, N.J.; Iacozza, J. Long-term trends in the population ecology of polar bears in western Hudson Bay in relation to climate change. *Arctic* **1999**, *52*, 294–306. [CrossRef]
5. Stirling, I. *Polar Bears: The Natural History of a Threatened Species*; Fitzhenry and Whiteside: Markham, ON, Canada, 2011; p. 352.
6. Aars, J.; Marques, T.A.; Buckland, S.T.; Andersen, M.; Belikov, S.; Boltunov, A.; Wiig, O. Estimating the Barents Sea polar bear subpopulation size. *Mar. Mammal Sci.* **2009**, *25*, 35–52. [CrossRef]
7. Obbard, M.E.; Middel, K.R.; Stapleton, S.; Thibault, I.; Brodeur, V.; Jutras, C. *Estimating Abundance of the Southern Hudson Bay Polar Bear Subpopulation using Aerial Surveys, 2011 and 2012*; Ontario Ministry of Natural Resource, Science and Research Branch: Peterborough, ON, Canada, 2013.
8. Stapleton, S.; Atkinson, S.; Hedman, D.; Garshelis, D. Revisiting western hudson bay: Using aerial surveys to update polar bear abundance in a sentinel population. *Biol. Conserv.* **2014**, *170*, 38–47. [CrossRef]
9. Stapleton, S.; Peacock, E.; Garshelis, D.; Atkinson, S. *Foxe Basin Polar Bear Aerial Survey, 2009 and 2010: Final Report*; Government of Nunavut: Iqaluit, NU, Canada, 2012.
10. Stapleton, S. Alternative Methods for Monitoring Polar Bears in the North American arctic. Ph.D. Thesis, University of Minnesota, Minneapolis, MN, USA, 2013.
11. Stapleton, S.; LaRue, M.; Lecomte, N.; Atkinson, S.; Garshelis, D.; Porter, C.; Atwood, T. Polar bears from space: Assessing satellite imagery as a tool to track Arctic wildlife. *PLoS ONE* **2014**, *9*, e101513. [CrossRef] [PubMed]
12. Kerbes, R.H.; Meeres, K.M.; Alisaukas, R.T.; Caswell, F.D.; Abraham, K.F.; Ross, R.K. *Surveys of Nesting Mid-Continent Lesser Snow Geese and Ross's Geese in Eastern and Central Arctic Canada, 1997–1998*; Technical Report Series No. 447; Canadian Wildlife Service, Prarie and Northern Region: Saskatoon, Saskatchewan, 2006.
13. Conn, P.B.; Hoef, J.M.V.; McClintock, B.T.; Moreland, E.E.; London, J.M.; Cameron, M.F.; Dahle, S.P.; Boveng, P.L. Estimating multispecies abundance using automated detection systems: Ice-associated seals in the Bering Sea. *Methods Ecol. Evolut.* **2014**, *5*, 1280–1293. [CrossRef]
14. Guinet, C.; Jouventin, P.; Malacamp, J. Satellite remote sensing in monitoring change of seabirds: Use of Spot Image in king penguin population increase at the Ile aux Cochons, Crozet Archipelago. *Polar Biol.* **1995**, *15*, 511–515. [CrossRef]

15. Barber-Meyer, S.M.; Kooyman, G.L.; Ponganis, P.J. Estimating the relative abundance of emperor penguins at inaccessible colonies using satellite imagery. *Polar Biol.* **2007**, *30*, 1565–1570. [CrossRef]
16. Fretwell, P.; LaRue, M.; Morin, P.; Kooyman, G.L.; Wienecky, B.; Ratcliffe, N.; Fox, A.; Fleming, A.; Porter, C.; Trathan, P. An emperor penguin population estimate: The first global, synoptic survey of a species from space. *PLoS ONE* **2012**, *7*, e33751. [CrossRef]
17. LaRue, M.; Rotella, J.; Garrott, R.; Siniff, D.; Ainley, D.; Stauffer, G.; Porter, C.; Morin, P. Satellite imagery can be used to detect variation in abundance of Weddell seals (Leptonychotes weddellii) in Erebus Bay, Antarctica. *Polar Biol.* **2011**, *34*, 1727–1737. [CrossRef]
18. Platonov, N.G.; Mordvintsev, I.N.; Rozhnov, V.V. The possibility of using high resolution satellite imagery for detection of marine mammals. *Biol. Bull.* **2013**, *40*, 197–205. [CrossRef]
19. Lavigne, D.M.; Øritsland, N.A. Black polar bears. *Nature* **1974**, *251*, 218–219. [CrossRef]
20. Lavigne, D.M.; Øritsland, N.A. Ultraviolet photography: A new application for remote sensing of mammals. *Can. J. Zool.* **1974**, *52*, 939–941. [CrossRef] [PubMed]
21. Øritsland, N.A.; Lavigne, D.M. Radiative surface temperatures of exercising polar bears. *Comp. Biochem. Physiol. A Physiol.* **1976**, *53*, 327–330. [CrossRef]
22. Grojean, R.E.; Sousa, J.A.; Henry, M.C. Utilization of solar radiation by polar animals: An optical model for pelts. *Appl. Opt.* **1980**, *19*, 339–346. [CrossRef] [PubMed]
23. Burn, D.M.; Udevitz, M.S.; Speckman, S.G.; Benter, R.B. An improved procedure for detection and enumeration of walrus signatures in airborne thermal imagery. *Int. J. Appl. Earth Obs. Geoinf.* **2009**, *11*, 324–333. [CrossRef]
24. Brooks, J.W. Infrared scanning for polar bear. In Proceedings of the International Conference on Bear Research and Management, Calgary, AB, Canada, 6–9 November 1972; pp. 138–141.
25. Amstrup, S.C. Polar bear, Ursus maritimus. In *Wild Mammals of North America: Biology, Management, and Conservation*; Feldhamer, G.A., Thompson, B.C., Chapman, J.A., Eds.; Johns Hopkins University Press: Baltimore, MD, USA, 2003; pp. 587–610.
26. Watts, P.D. Ecological Energetics of Denning Polar Bears and Related Species. Ph.D. Thesis, University of Oslo, Oslo, Norway, 1983.
27. Amstrup, S.C.; York, G.; McDonald, T.L.; Nielson, R.; Simac, K. Detecting denning polar bears with forward-looking infrared (FLIR) imagery. *Bioscience* **2004**, *54*, 337–344. [CrossRef]
28. Kimes, D.S.; Kirchner, J.A.; Newcomb, W.W. Spectral radiance errors in remote-sensing ground studies due to nearby objects. *Appl. Opt.* **1983**, *22*, 8–10. [CrossRef] [PubMed]
29. Price, J.C. How unique are spectral signatures. *Remote Sens. Environ.* **1994**, *49*, 181–186. [CrossRef]
30. Satellite Imaging Corporation. Available online: http://www.satimagingcorp.com/satellite-sensors/ (accessed on 16 March 2016).
31. Eastman Kodak Company. *KODAK Double-X Aerographic Film 2405*; Eastman Kodak Company: Rochester, NY, USA, 2005.
32. Downing, S.C. Color changes in mammal skins during preparation. *J. Mammol.* **1945**, *26*, 128–132. [CrossRef]
33. Davis, A.K.; Woodall, N.; Moskowitz, J.P.; Castleberry, N.; Freeman, B.J. Temporal change in fur color in museum specimens of mammals: Reddish-brown species get redder with storage time. *Int. J. Zool.* **2013**, *2013*, 876347. [CrossRef]
34. DeMaster, D.P.; Stirling, I. Ursus maritimus. *Mamm. Species* **1981**, *145*, 1–7. [CrossRef]
35. Gerland, S.; Winther, J.G.; Orbaek, J.B.; Ivanov, B.V. Physical properties, spectral reflectance and thickness development of first year fast ice in Kongsfjorden, Svalbard. *Polar Res.* **1999**, *18*, 275–282. [CrossRef]